

# Design and Control of Tensegrity Robots for Locomotion

Chandana Paul, *Member, IEEE*, Francisco J. Valero-Cuevas, *Member, IEEE*, and Hod Lipson, *Member, IEEE*

**Abstract**—The static properties of tensegrity structures have been widely appreciated in civil engineering as the basis of extremely lightweight yet strong mechanical structures. However, the dynamic properties and their potential utility in the design of robots have been relatively unexplored. This paper introduces robots based on tensegrity structures, which demonstrate that the dynamics of such structures can be utilized for locomotion. Two tensegrity robots are presented: TR3, based on a triangular tensegrity prism with three struts, and TR4, based on a quadrilateral tensegrity prism with four struts. For each of these robots, simulation models are designed, and automatic design of controllers for forward locomotion are performed in simulation using evolutionary algorithms. The evolved controllers are shown to be able to produce static and dynamic gaits in both robots. A real-world tensegrity robot is then developed based on one of the simulation models as a proof of concept. The results demonstrate that tensegrity structures can provide the basis for lightweight, strong, and fault-tolerant robots with a potential for a variety of locomotor gaits.

**Index Terms**—Genetic algorithms, locomotion, tensegrity.

## I. INTRODUCTION

THE conventional design of locomotor robots has been based on a series of rigid links connected by prismatic or revolute joints, actuated using electric motors or pneumatic or hydraulic actuators. The majority of legged robots have been based on this design [20], [39], although, in some robots, geared towards dynamic gait, the actuators have been supplemented with series elastic elements [37] or replaced with passive compliance [4], [38]. In this study, the goal was to depart from this conventional design methodology and explore a new paradigm in the mechanical design of locomotor robots, based on the concept of tensegrity. Tensegrity structures are volumetric mechanical structures composed of a set of separate rigid elements connected by a continuous network of tensional elements. Due to an intricate balance between the tensile and compression forces in the structure, the structure is maintained at equilibrium. When a moderate deforming force is applied at one point of the structure, only a transient change is effected in the global form, after which the structure once again returns to its equilibrium configuration. Only in some cases, can the

structure be “locked” into a two-dimensional (2-D) form with a specific sequence of forces.<sup>1</sup>

Tensegrity structures were first invented by Snelson in 1948 and formally patented by Buckminster Fuller in 1962 [16], who coined the word tensegrity as an abbreviation of *tensile integrity*. The general definition of a tensegrity structure is a structure that maintains a stable volume in space through the use of discontinuous compressive elements (struts) connected to a continuous network of tensile elements (cables) [35]. However, there is some disagreement regarding the more specific characteristics that define a tensegrity structure. For example, according to Connelly and Black [8], in a tensegrity structure, vertices connected by a cable may be arbitrarily close, but they may not be further than the length of the cable joining them. This definition works well when the cables are made of inelastic material. However, when elastic cables are used, the vertices may be further apart than the remaining length of the cable, if appropriate force is applied. Other definitions have variations in the level of spatial proximity allowed between the struts. In the definition of a *class I* tensegrity structure [3], the struts cannot share common vertices, that is, they must be physically separated in space. However, the definition of a *class II* tensegrity structure allows more than one strut to originate from a vertex. Finally, although the canonical form of a tensegrity structure is composed of rigid struts and tensile cables, tensegrity structures also exist in which the struts are elastic and connected by cables or sheets of material.<sup>2</sup>

Due to their design, tensegrity structures have been discovered to have the ability to form the basis of lightweight and strong mechanical structures using little material. This has gained them widespread popularity in architectural design for structures such as bridges and geodesic domes [19]. Their utility has also been recognized for the design of lightweight space structures such as deployable masts [17] and reflector antennas [27], [49].

Numerous theoretical investigations of the static properties of tensegrity structures have been undertaken. In particular, the problem of *form finding*, determining the geometrical configuration of a tensegrity structure, has received much attention. Early structures developed by Fuller and Snelson used convex polyhedra as the basis for form-finding. This approach resulted in various configurations which were summarized by Pugh [35]. More recently, other methods have been developed which include the use of nonlinear programming [36], dynamic relaxation [32], symmetry [7], [8], volume maximization [56], and calculation of force density [29], [41], [51]. A good review of these and other form-finding methods can be found in [50].

Manuscript received February 11, 2005; revised July 19, 2005. This paper was recommended for publication by Associate Editor J. Angeles and Editor I. Walker upon evaluation of the reviewers' comments. This work was supported by the U.S. DCI Postdoctoral Research Fellowship Program under Award NMA501-03-1-2013. This paper was presented in part at ICAR 2005, Seattle, WA, July 2005, and IROS 2005, Edmonton, AB, Canada, August 2005.

The authors are with the Mechanical and Aerospace Engineering Department, Cornell University, Ithaca, NY 14853 USA (e-mail: cp228@cornell.edu).  
Digital Object Identifier 10.1109/TRO.2006.878980

<sup>1</sup>This is often used for low-volume stowage and transportation.

<sup>2</sup>The pop-up tent is a good example of such a tensegrity structure.

In addition to the static characteristics, the mechanics and motion control of tensegrity structures have also been investigated to some extent. De Jager and Skelton have studied the placement of sensors and actuators on planar tensegrity models [11] and integrated design of topology and control [12]. Kanchanasaratool and Williamson have developed a constrained particle dynamic model, assuming zero mass struts, and used the input–output mapping of this model to formulate a neural-network-based inversion for path tracking [24], [25]. Domer *et al.* have studied the use of the stochastic search techniques simulated annealing and probabilistic global search for shape control [13]. Sultan *et al.* have investigated nonlinear control for a tensegrity-based flight simulator [46]. Only a few groups have studied motion control directly in the context of robotics. Aldrich *et al.* have developed methods for trajectory tracking in a tensegrity-based robotic manipulator [2], and Masic and Skelton have considered self-propelled tensegrity towers using transversal wave shape control [55].

To our knowledge, the use of tensegrity in the context of locomotor robots has not been previously implemented. This is potentially a considerable oversight as, in some respects, tensegrity structures closely resemble the structural architecture of biological systems with the ability to locomote. It has been shown that the cytoskeleton of a cell is similar to a tensegrity structure [22], [23], and numerous single-celled organisms are known to locomote. Furthermore, tensegrity structures are also similar to musculo-skeletal systems of highly successful land-based animals in their use of tensile elements. Cats, which can jump several meters in height without causing damage to their structure, and cheetahs, which can achieve maximum speeds of over 60 mph, are able to perform these incredible feats due to the intricate incorporation of tensional elements in their musculo-skeletal system [52]. Their musculo-skeletal systems are made up of rigid links (bones) which are connected by tensile elements (tendons) with contractive elements (muscle fibers) in series. The tensile elements maintain the integrity of the form and store energy, making it possible to sustain large impact forces and transfer energy from one bound to the next. Due to this architectural equivalence, it is likely that tensegrity structures can provide a suitable basis for locomotion.

Although tensegrity robots and other structures that utilize tension such as cable-suspended robots [1] have been considered in the past, their dynamics have been treated as an engineering liability. Various attempts have been made to overcome or eliminate them, using mechanical solutions such as tendons to stiffen the structure [5] or control solutions to cancel out the natural dynamics [2], [34]. This study is the first to consider the dynamics an asset and utilize them. The dynamics allow for the storage and release of energy which facilitates locomotion.

Tensegrity structures also provide benefits in terms of weight and strength-to-weight ratio. Recent years have seen a trend towards mobile robot applications in autonomous space exploration, operations in hazardous environments, military operations, and human assistive functions. As the financial costs of transportability and the energetic costs of mobility are key issues in these areas, they could greatly benefit from advances in lightweight design techniques that do not require the sacrifice of strength or functionality.

In pursuit of these potential benefits, our study addresses the design of robots using tensegrity and the motion control of these structures for locomotion. The tensegrity structures described in this paper do not resemble the morphologies of conventional legged robots and cannot be easily recognized as biomimetic bipeds, quadrupeds, or hexapods. Nonetheless, their mode of locomotion can be classified as legged, as it involves a sequence of discrete foot contact events. This is in contrast to mobile robots which use wheels for continuous rolling (or sliding) contact.

Tensegrity structures can be made in a variety of ways, and each variation is likely to be interesting in its own right. However, as a preliminary step, this paper addresses the subset of tensegrity structures in which cables are elastic and struts are rigid, disconnected, and spatially separated. Within the constraints of this definition, there are also variations depending on the number of cables that originate at each vertex. Here, we focused on structures which have exactly three cables originating at each vertex.

For the control of the tensegrity robots for locomotion, precise trajectory tracking was not considered a high priority. Instead, the primary focus was the production of gait, defined as the generation of rhythmic motions which lead to nonzero movement of the center of mass [30]. McIsaac and Ostrowski developed an analytical approach to determine higher order patterns of control inputs which could lead to periodic motions in mechanisms with nonholonomic constraints. However, in this paper, an alternative, computational approach was employed to converge on periodic patterns of actuation for locomotion, which did not require assumptions on the constraints. This method is used for the control of two tensegrity robots, TR-3 and TR-4, which are based on tensegrity prisms of three and four struts, respectively. The results demonstrate successful production of static and dynamic gait patterns in both robots and robustness to actuator failures. The results show that even simple tensegrity structures can harbor the potential for dynamic gait production and thus suggests the utility of tensegrity for the design of land-based locomotor robots.

## II. DYNAMICS

The dynamics of tensegrity structures have been studied in previous work. Kanchanasaratool and Williamson [24] have developed a constrained particle dynamic model assuming zero mass struts, using the Lagrange method. Skelton *et al.* [42], Sultan [45], and Aldrich *et al.* [2] have developed more complete models including mass and inertial properties. Skelton *et al.* have instantiated the struts as point masses located at the endpoints to avoid the use of angular velocities and derived an expression for strut accelerations in the shell class of tensegrity structures. Sultan has represented the struts as rigid bodies and modeled the dynamics in the absence of gravity using the Lagrange method. Aldrich *et al.* have used a model of a serial link chain adapted to the geometry of a tensegrity structure and derived the dynamics using the Lagrange method for the control of a robot manipulator.

For the class of tensegrity structures used in this work, the Newton–Euler method is suitable for the development of the equations of motion. Tensegrity structures with elastic cables do not have rigid joints to generate constraints, and, thus, in

essence, each strut can be considered a free body with a set of forces acting on it. Thus, the Newton–Euler method is more amenable to the analysis of such structures as, in this method, every rigid body is treated as a free body.

This method can be used to develop the equations of motion for an actuated tensegrity. In general, if a tensegrity structure has  $n$  struts, in three dimensions, each strut has six degrees of freedom (DOF). These include three position variables  $[x_i, y_i, z_i]$  and three orientation variables  $[\theta_i, \phi_i, \psi_i]$  for the  $i$ th strut, the latter of which specify angles with respect to the  $X$ -,  $Y$ -, and  $Z$ -axes, respectively. Thus, the state vector for a system of  $n$ -struts is a vector  $q \in \mathbb{R}^{6n}$ , such that

$$q = [x_1, y_1, z_1, \theta_1, \phi_1, \psi_1, \dots, x_n, y_n, z_n, \theta_n, \phi_n, \psi_n]. \quad (1)$$

Depending on the configuration of the tensegrity structure, every strut end is connected to three elastic cables that exert forces on the rigid struts. The set of cable forces is  $\mathbf{F}_C = [\mathbf{F}_{C_1}, \mathbf{F}_{C_2}, \dots, \mathbf{F}_{C_{2m}}]$ , where  $m$  is the number of cables. Note that there are twice as many cable forces as cables, as each cable will produce two force vectors in equal and opposite directions, one on each strut to which it is attached. Each cable force magnitude is calculated as follows:

$$F_i = k (\|\mathbf{r}_j - \mathbf{r}_k\| - l_{c_i}^r) - c \left( \frac{d\|\mathbf{r}_j - \mathbf{r}_k\|}{dt} \right) \quad (2)$$

where  $\mathbf{r}_j$  and  $\mathbf{r}_k$  are the position vectors of the strut ends to which the cable is attached and  $l_{c_i}^r$  is the rest length of the cable which produces  $F_i$ . The force vector  $\mathbf{F}_{C_i}$  produced at the strut end represented by position vector  $\mathbf{r}_j$  due to the cable connected between strut ends  $\mathbf{r}_j$  and  $\mathbf{r}_k$  is

$$\mathbf{F}_{C_i} = F_i \cdot (\mathbf{r}_k - \mathbf{r}_j). \quad (3)$$

In addition to the cable forces, the rigid struts also experience occasional contact forces from the ground. Assuming that, during normal behavior, only one end of a strut contacts the ground at any time, the set of ground forces is  $\mathbf{F}_G = [\mathbf{F}_{G_1}, \mathbf{F}_{G_2}, \dots, \mathbf{F}_{G_n}]$ . These forces are nonzero only upon contact and can be calculated according to a standard spring-damper-based ground model [48].

Thus, the Newton–Euler Equations for the tensegrity structure can be written in the following generalized form:

$$\mathbf{A}(\mathbf{q})\ddot{\mathbf{q}} = \mathbf{B}(\mathbf{q}, \dot{\mathbf{q}}, \mathbf{F}_G, \mathbf{F}_C) \quad (4)$$

where  $\mathbf{A}(\mathbf{q})$  is the inertia matrix.

This parametric formalization can be used to represent not only tensegrity robots but also biological musculo-skeletal systems and standard robotic structures. Thus, it yields a general framework that can be used to compare the performance of various natural and artificial morphologies.

### III. IMPLEMENTATION

The tensegrity structures were implemented in the open dynamics engine (ODE) simulation environment, which provides

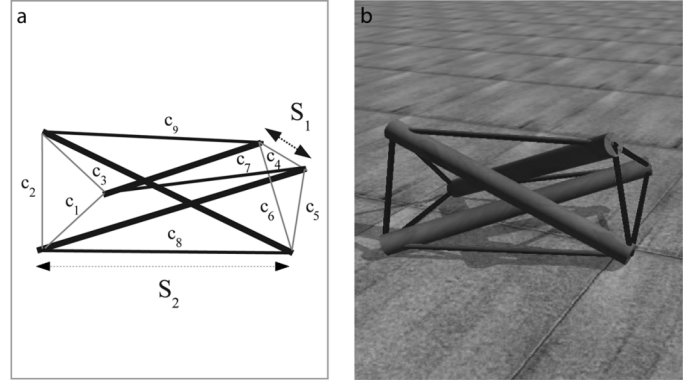


Fig. 1. (a) Schematic of the three-prism tensegrity structure. The thick black lines indicate the struts. The thin gray lines indicate the cables at the two ends of the prism. These are of length  $S_1$ . The thin black lines indicate the transverse cables connecting the two sides of the prism. These are of length  $S_2$ . (b) The robot TR-3, based on the three-prism tensegrity structure, in simulation.

physics-based simulation of rigid body motion. It includes implementation of the frictional characteristics of ground surfaces, gravity, and the dynamics of multilink rigid bodies composed of various types of joints.

The struts of the tensegrity structures were implemented as rigid cylindrical bodies. The outer surfaces of the struts had elastic contact properties such that, when in contact with another surface, they generated forces which resisted penetration. The cables, in contrast, were implemented as virtual objects which were massless and volumeless and did not have any contact characteristics. Each cable was represented by a collinear pair of forces, one of which is applied at the end of each strut to which the cable is attached. The magnitude of the force  $F$  was based on a spring-damper model

$$F = \begin{cases} \frac{k}{l_o}(l - l_o) - c\frac{dl}{dt} & l - l_o > 0 \\ 0 & l - l_o \leq 0 \end{cases} \quad (5)$$

where  $l$  is the current distance between the relevant strut endpoints,  $l_o$  is the spring rest length,  $k$  is the spring coefficient, and  $c$  is the damping coefficient. The forces were applied along the instantaneous location of the line joining the end points of the two struts to which the cable was attached. If the endpoints were further than the rest length of the cable, the forces would be positive, but, if they were closer, the forces would be zero, indicating a loss of cable tension. This was allowed to occur as it was a natural result of the dynamics being strongly excited during dynamic locomotion.

Figs. 1 and 2 show the morphology of the TR-3 and TR-4 robots, and Tables I and II show the values of the parameters used in the implementation of these robots, respectively.

#### A. Actuation

Three methods of actuation are possible in a tensegrity structure: strut-located, cable-located, and noncollocated actuation. In strut-located actuation, the actuators are responsible for altering the strut lengths. In cable-located actuation, the structure is modified by changing the effective rest length of the cables. In noncollocated actuation, actuation is applied between two struts, two cables, or a strut and a cable.

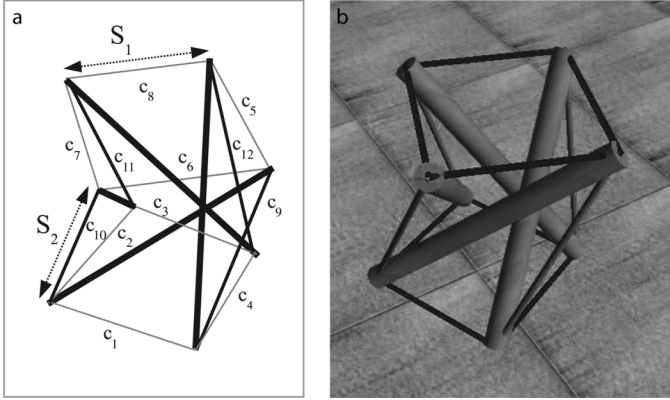


Fig. 2. (a) Schematic of the four-prism tensegrity structure. The thick black lines indicate the struts. The thin gray lines indicate the cables at the two ends of the prism. These are of length  $S_1$ . The thin black lines indicate the transverse cables connecting the two sides of the prism. These are of length  $S_2$ . (b) The robot TR-4, based on the four-prism tensegrity structure, in simulation.

TABLE I  
VALUES OF PARAMETERS FOR THE TR-3 ROBOT

strut length	1.01 m
cable spring constant $k$	0.70 N/m
cable damping constant $c$	10.00 Ns/m
cable rest length $S_1^o$ (short)	0.35 m
cable rest length $S_2^o$ (long)	0.44 m
equilibrium cable length $S_1$	0.44 m
equilibrium cable length $S_2$	0.88 m

TABLE II  
VALUES OF PARAMETERS FOR THE TR-4 ROBOT

strut length	1.00 m
cable spring constant $k$	0.70 N/m
cable damping constant $c$	10.00 Ns/m
cable rest length $S_1^o$ (short)	0.24 m
cable rest length $S_2^o$ (long)	0.23 m
equilibrium cable length $S_1$	0.51 m
equilibrium cable length $S_2$	0.80 m

Cable-collocated actuation was selected for both the TR-3 and TR-4 robots. This is similar to prior work on motion control of a tensegrity structure for a flight simulator in which the control variables were the rest lengths of the cables [46]. On the TR-3 and TR-4 robots, the cables were located on the longitudinal cables of the prisms as indicated in Figs. 1 and 2 by the black cables ( $c_7 - c_9$  in TR-3 and  $c_9 - c_{12}$  in TR-4). The actuators applied force on the structure by effecting a change in the rest length of these cables. For the TR-3, the maximum change in the cable length was 0.10 m and, for the TR-4 robot, the maximum change was 0.06 m. The control of the robot was accomplished by periodically changing the rest lengths of these cables between the maximum and minimum values. In simulation, this change was considered to be instantaneous.

#### IV. CONTROLLER DESIGN USING A GENETIC ALGORITHM

Each actuator was contracted once during each gait cycle. The controller determined the phase of the gait cycle at which each actuator was activated, the duration of contraction, and the amplitude of contraction independently for each actuator. It also determined the overall period of the gait.

Thus, the relevant parameters in the control were:

$\lambda$	period of the gait cycle;
$\alpha_i$	amplitude of actuation for each cable;
$\phi_i$	phase of onset of actuation for each cable;
$\delta_i$	duration of actuation for each cable;
$l_{c_i}^r$	current rest length of each cable;
$l_{c_i}^o$	original rest length of each cable;
$t_i^o$	time of onset in each cycle;
$t$	time.

The controller had the following algorithmic form.

*In each time step, for each cable  $c_i$*

$$if\ t \bmod \lambda = \phi_i, \text{ set } t_i^o = t$$

$$l_{c_i}^r = \begin{cases} l_{c_i}^o - \alpha_i l_{c_i}^o : & t_i^o < t < t_i^o + \delta_i \\ l_{c_i}^o : & t > t_i^o + \delta_i. \end{cases}$$

According to this, actuation of a cable was initiated when  $t$  was at the phase of onset specified by the parameter  $\phi_i$ . At this point, the parameter  $t_i^o$  was initialized to the value of  $t$ . Subsequently, the cable was activated for  $\delta_i$  time steps and then deactivated for the rest of the gait cycle.

A genetic algorithm [31] was used to optimize the controller for locomotion by performing a computational search through the parameter space defined by  $\lambda$ ,  $\alpha_i$ ,  $\phi_i$ , and  $\delta_i$ . Each agent in the population had a genome string with floating point values between 0 and 1. The first value in the string  $p$  encoded the period of the gait cycle. The rest of the genome string was composed of triples  $[a_i, o_i, d_i]$  encoding the amplitude, phase, and duration for each cable. The parameters  $\lambda$ ,  $\alpha_i$ ,  $\phi_i$ , and  $\delta_i$  were determined from these values as follows:

$$\lambda = \lambda_{\min} + [p(\lambda_{\max} - \lambda_{\min})]$$

$$\alpha_i = [a_i \alpha_{\max}]$$

$$\phi_i = [o_i \lambda]$$

$$\delta_i = [d_i \lambda]$$

where  $\lambda_{\max} = 500$ ,  $\lambda_{\min} = 200$ , and  $\alpha_{\max} = 0.10$ .

A fixed-length genetic algorithm was used to evolve the controllers. Each run of the genetic algorithm was conducted for 200 generations, using a population size of 200. At the end of each generation, the 100 most fit genomes were preserved; the others were deleted. Tournament selection with a tournament size of three was employed to probabilistically select genotypes from among those remaining for mutation and crossover. Twenty-five pairwise one-point crossings produced 50 new genotypes: the remaining 50 new genotypes were mutated copies of genotypes from the previous generation. The mutation rate was set to generate an average of  $n$  mutations for each new genome created, where  $n$  was defined as a function of the genome length  $g_l$ , as  $n = g_l/11$ . Mutation involved the replacement of a single value with a new random value. The floating-point values were rounded to two decimal places and thus ranged between 0.00 and 1.00. For the TR-3 robot, the genome had 10 values and, for the TR-4 robot, 13 values. The first value represented the period of the gait cycle, and the rest

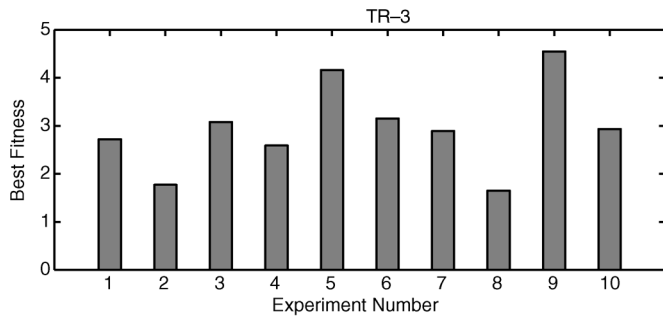


Fig. 3. Results: best fitness achieved in each of the ten evolutionary experiments with the TR-3 robot.

of the genome consisted of triples representing phase, duration, and amplitude of actuation for the three actuated cables.

During evolution, each individual was evaluated for 10 000 time steps of the dynamics simulation, where each time step corresponded to 0.001 s. The initial condition for each individual at the first time step was at position  $[0, 0]$  in the  $x$ - $y$  plane. The fitness of the individual was determined at the end of the evaluation period, and was considered to be the distance traveled in the  $y$ -direction with respect to the origin.

## V. RESULTS

### A. TR-3

Ten evolutionary optimizations were performed to obtain controllers for the TR-3 robot in simulation. The best fitness achieved in each of these runs is shown in Fig. 3. In most of the experiments, controllers were evolved, which led to nonzero movement of the center of mass in each cycle, although some were more effective than others. The fitness was a measure of the distance traveled in the forward direction in 10 s. The final fitnesses in the experiments ranged between 1.6–4.6 m and the average fitness was  $2.95 \pm 0.91$  m.

The gaits achieved in the various runs varied in their pattern of actuation and, as a result, in their movement pattern. Some gaits were slow and static, similar to an inchworm gait. Experiment 4 yielded such a gait pattern. The pattern of actuation employed in this gait can be seen in the graphs of cables forces of the actuated cables in Fig. 4. An instantaneous increase in cable force corresponded to activation of the actuator, which lead to contraction of the cable. Conversely, an instantaneous decrease in cable force corresponded with deactivation of the actuator. Referring back to Fig. 1, cables  $c_7$  and  $c_8$  are the actuated cables close to the ground, and cable  $c_9$  is the one on top. Thus, as the force graphs in Fig. 4 show, the gait is produced roughly by activating the bottom two cables  $c_7$  and  $c_8$  for equal durations one after the other, while keeping the top actuator  $c_9$  active, and then relaxing all three actuators. If the actuators are labeled from front to back in Fig. 1,  $c_8$  is actuator 1,  $c_9$  is actuator 2, and  $c_7$  is actuator 3. The pattern of actuation can then be written as a sequence of binary states  $[s_1, s_2, s_3]$ , where  $s_i$  is a binary value corresponding to the state of actuator  $i$ . 0 corresponds to the actuator being relaxed, and 1 corresponds to the actuator being activated (contracted). Thus, the pattern of actuation in this gait can be seen a repeated loop through the states  $[0, 1, 1]$ ,

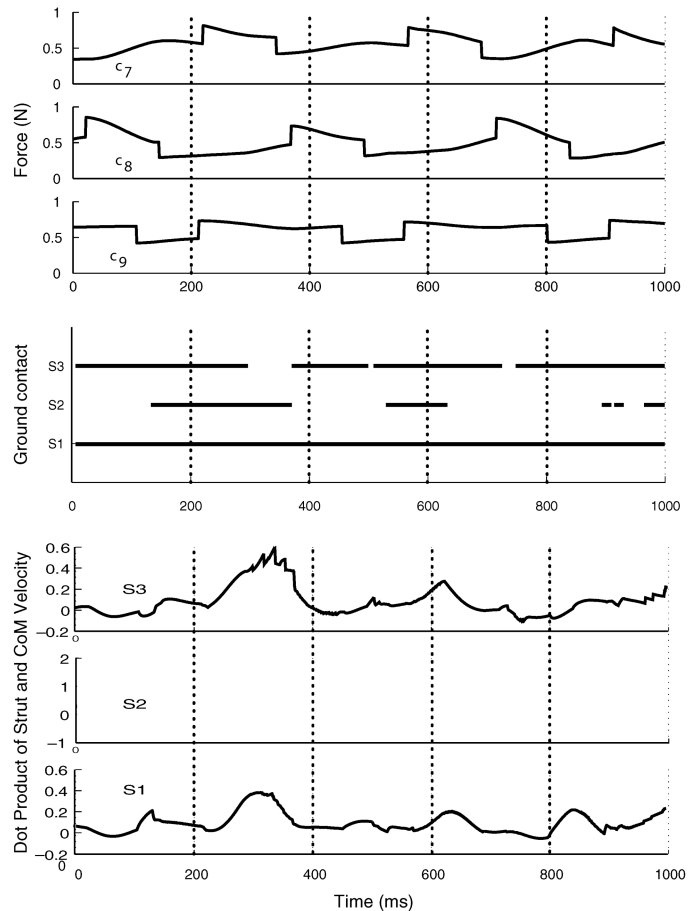


Fig. 4. TR-3, Experiment 4. Top: cable forces plotted as a function of time for 1000 ms, from top to bottom for the actuated cables  $c_7$ – $c_9$  (Fig. 1), respectively. Middle: ground contact information plotted for struts  $S_1$ ,  $S_2$  and  $S_3$  for 1000 ms. Dark portions of the lines indicate that a strut is in contact with the ground, and white portions indicate absence of ground contact. Bottom: dot product of the strut velocities with the velocity of the center of mass. These graphs indicate the contribution of the struts to the forward movement of the body.

$[1, 1, 0]$ ,  $[1, 0, 0]$ ,  $[0, 0, 0]$ . The cable forces have been plotted for 1000 ms (Fig. 4) and in this duration of time, approximately three loops through this sequence of states is performed. Thus, the frequency of the gait cycle is approximately 3 Hz.

The middle set of graphs in Fig. 4 show the corresponding foot contact data. It can be seen that the actuation pattern gives rise to a slow, relatively static gait in which all three contact points are on the ground for large parts of the gait cycle. The gait can be understood as the robot dragging two of its struts along, using the third as a pick axe. The contact data shows that the gait pattern is not perfectly periodic, unlike the pattern of control inputs. However, a rough periodicity can be observed if the data is plotted for 10 s.

The lower set of graphs in Fig. 4 plot the dot product of the velocity vector of each strut, with the velocity vector of the center of the mass of the robot. These graphs indicate the contribution of each strut to the forward movement of the body. The graphs show that the three struts alternately contribute to forward movement.  $S_3$  and  $S_2$  make larger contributions when they are not in contact with the ground, whereas  $S_1$  contributes while being in contact with ground.

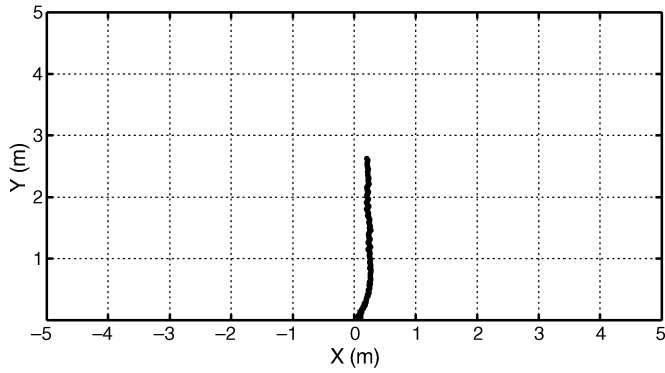


Fig. 5. TR-3, Experiment 4: the trajectory of the center of mass of the TR-3 robot plotted for 10 s of operation time.

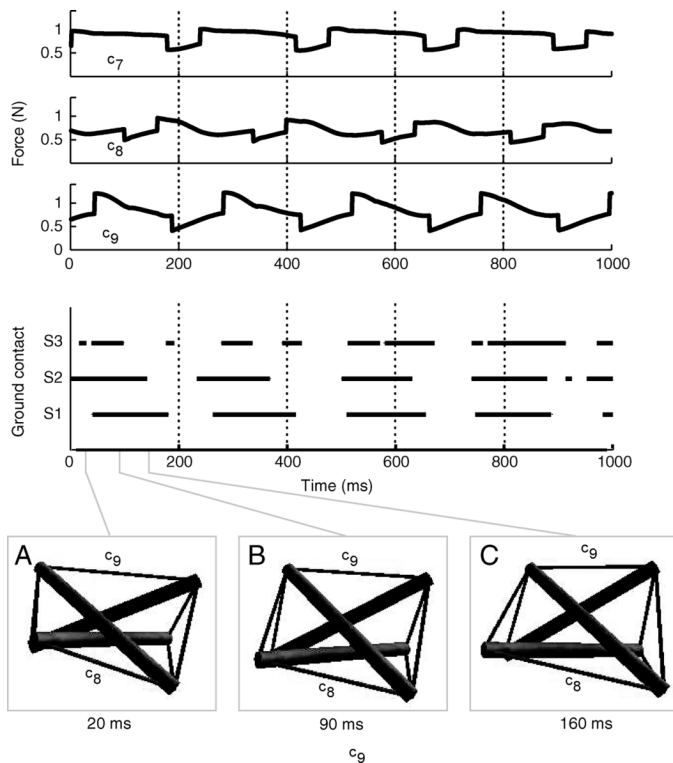


Fig. 6. TR-3, Experiment 9: Top: cable forces as function of time for 1000 ms, plotted from top to bottom for the actuated cables  $c_7$ – $c_9$  (Fig. 1), respectively. (Middle) ground contact information plotted for struts  $S_1$ ,  $S_2$  and  $S_3$  for 1000 ms. Dark portions of the lines indicate that a strut is in contact with the ground, and white portions indicate absence of ground contact. Bottom: configuration of the robot in three different phases of the gait cycle.

The position of the center of mass of the robot over 10 s is plotted in Fig. 5. The trajectory is curved in the initial transient phase, but then tracks a straight line. The slight aperiodic nature of the gait is apparent on close observation, in that not every step produces exactly the same change in the position of the center of mass. However, it is nonetheless effective in transporting the robot at an approximate forward speed of 0.26 m/s.

In contrast, the outcome of Experiment 9 was very different. The middle set of graphs in Fig. 6 which show the pattern of foot contact data for 1000 ms indicate that the gait was much more

dynamic and included flight phases in which all three contact points left the ground during certain phases of the gait cycle. The movement could be characterized as a bounding gait and was also more periodic than the previous example.

The actuation pattern that led to this gait can be observed in the graph of cables forces in Fig. 6. At the outset, it can be seen that cables  $c_7$  and  $c_8$  have a greater duty cycle in this gait, leading to greater energy input into the system. Also, a driving factor in this gait is the top cable  $c_9$ , which has a large change in length and force amplitude (Fig. 6). Following the controller through the sequence of binary states, the actuation pattern can be roughly characterized as  $[1\ 1\ 1]$   $[0\ 1\ 1]$   $[1\ 1\ 1]$   $[1\ 0\ 0]$   $[1\ 0\ 1]$ . In the 1000 ms plotted, slightly over four cycles of activation are observed. Thus, the frequency of the gait is approximately 4 Hz.

To understand the production of gait in more detail, the changes in configuration of the robot during one gait cycle are shown at the bottom of Fig. 6. The robot moves by alternating between the extreme configurations A and C, which mainly vary in the degree of contraction of the top cable  $c_9$ . This alternation leads to forward motion as can be seen in the sequence of still frames extracted from a video of the simulated robot moving in Fig. 7.

The position of the center of mass of the robot as a result of this gait is shown in Fig. 8. The trajectory has a slight eccentricity and does not perfectly track a straight line. However, the gait is fast, achieving a speed of 0.45 m/s.

## B. TR-4

Ten evolutionary optimizations were also performed to obtain controllers for the TR-4 robot in simulation. In contrast to the TR-3 robot, which was optimized for locomotion lying on its side, the TR-4 was optimized for locomotion standing on one end. The best fitness achieved in each of these runs is shown in Fig. 9. As can be seen, all the experiments successfully evolved locomotion. The fitnesses from the TR-4 robot were higher on average than those with the TR-3 robot and were in a range between 2.20–3.97 m. The average fitness was  $3.18 \pm 0.50$  m.

Experiment 1 produced a relatively fast gait with a fitness of 3.97. The pattern of actuation producing this gait can be seen in the graphs of cable forces of the actuated cables in Fig. 10. Here, the first cable  $c_9$  is activated for more than 90% of the gait cycle. The cables  $c_{10}$  and  $c_{11}$  alternate in their activation, such that  $c_{10}$  is active for 40% of the gait cycle and  $c_{11}$  for the remaining 60%. Cable  $c_{12}$  is activated at the same time as  $c_{11}$  and then deactivated shortly thereafter. The pattern of actuation can be characterized as a loop through the sequence of binary states  $[1\ 0\ 1\ 0]$   $[1\ 1\ 0\ 0]$   $[1\ 1\ 0\ 1]$   $[1\ 0\ 1\ 0]$   $[0\ 0\ 1\ 0]$ . This leads to a staggered pattern of foot contacts in which the struts make ground contact sequentially in the order  $S_4$ ,  $S_3$ ,  $S_2$ , and  $S_1$ . However, their ground contact phases overlap in time, and there are only brief durations in which all four struts are off the ground. It is interesting that this gait pattern is mostly static, as fast motion is usually associated with dynamic gait. In the 1000 ms plotted, six and a half periods of the gait cycle are produced, thus the frequency of the gait is approximately 6.5 Hz.

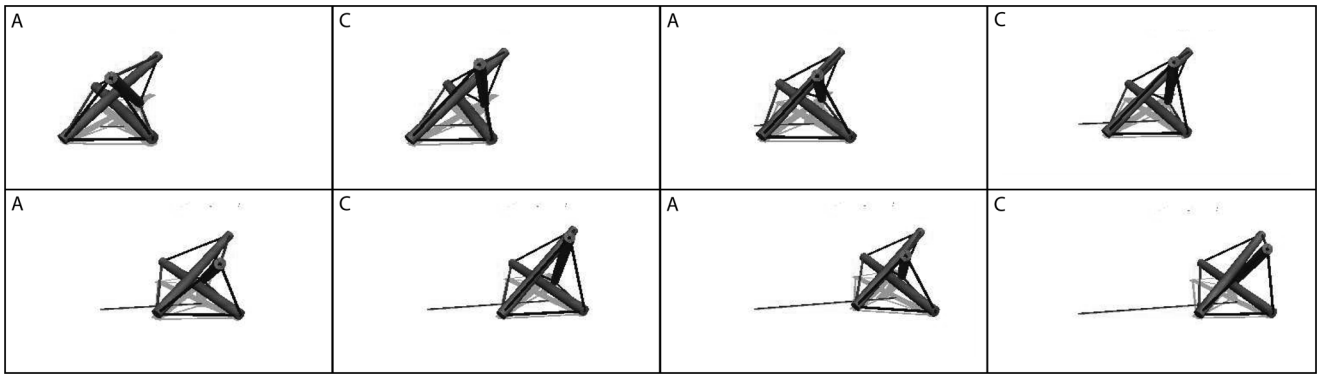


Fig. 7. Still frames extracted from video of the TR-3 robot locomoting in Experiment 4. The robot moves by alternating between configurations A and C, which are depicted in Fig. 6.

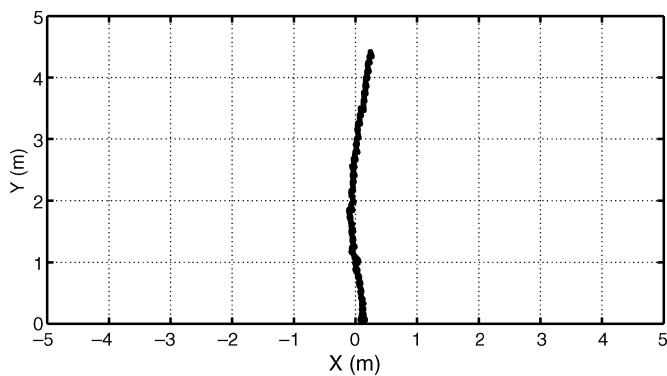


Fig. 8. TR-3, Experiment 9: the trajectory of the center of mass of the TR-3 robot, plotted for 10 s of operation time.

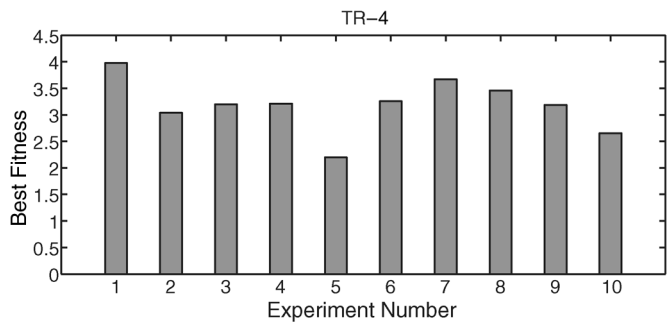


Fig. 9. Results: best fitnesses achieved in each of the ten evolutionary experiments with the TR-4 robot in simulation.

This is fast, compared with the other gaits presented, and may be a factor in the high performance of this gait.

The trajectory of the position of the center of mass of the robot is shown in Fig. 11. The trajectory has a distinct counterclockwise curvature. As the agents were rewarded for maximum distance traveled in the  $y$ -direction and not directly penalized for veering off a straight line course, some of the agents generated curved trajectories.

Experiment 5 achieved a slow but dynamic gait with a fitness of 2.20. The evolved pattern of actuation can be seen in the graph of cable forces in Fig. 12. Cables  $c_9$  and  $c_{12}$ , which are the two cables approximately facing the direction of motion, are both contracted at the same time. Notice that, for the example

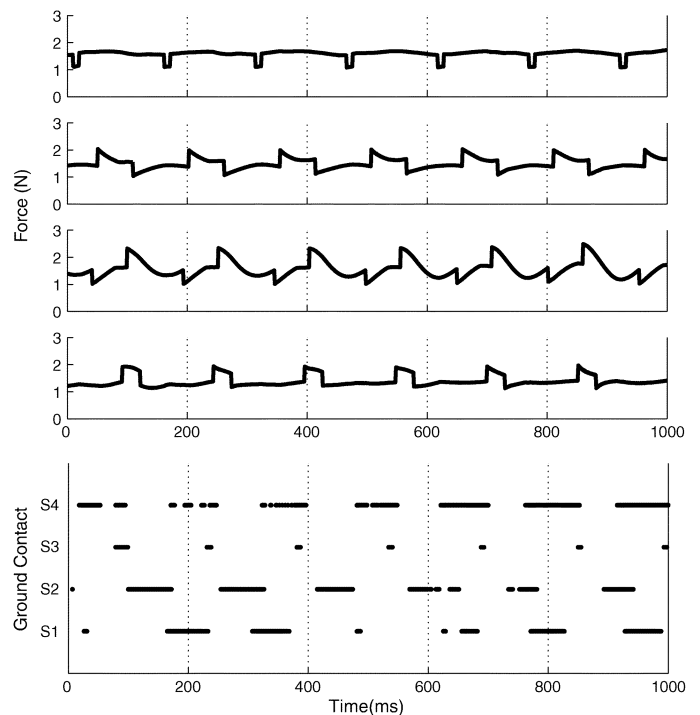


Fig. 10. TR-4, Experiment 1. Top: cable forces as a function of time for 1000 ms, plotted from top to bottom for the actuated cables  $c_9$ – $c_{12}$  (Fig. 2), respectively. Bottom: ground contact information plotted for struts  $S_1$ ,  $S_2$ ,  $S_3$  and  $S_4$  for 1000 ms. Dark portions of the lines indicate that a strut is in contact with the ground, and white portions indicate absence of ground contact.

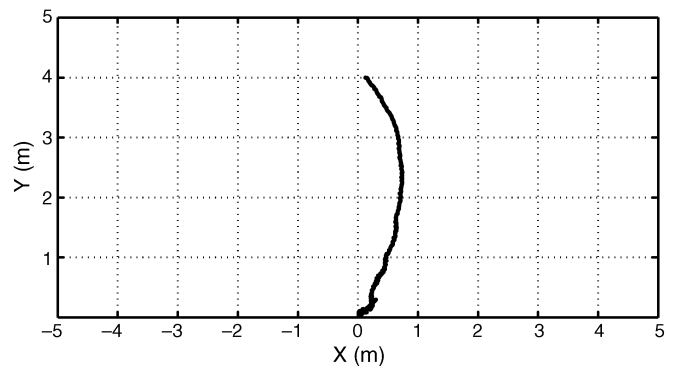


Fig. 11. TR-4, Experiment 1: the trajectory of the center of mass of the TR-4 robot is plotted for 10 s of operation time.

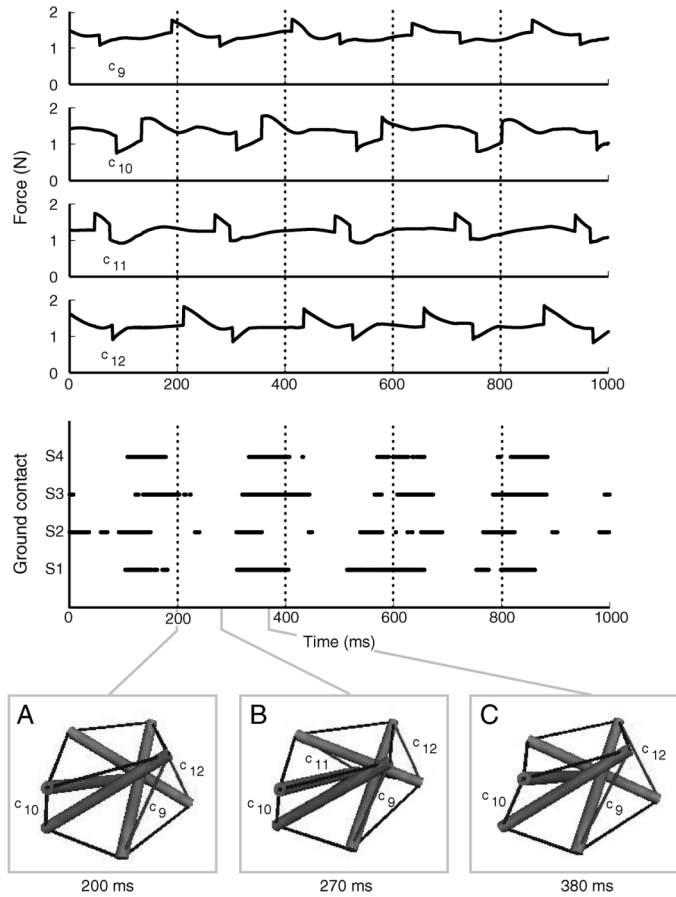


Fig. 12. TR-4, Experiment 5. Top: cable forces as function of time for 1000 ms, plotted from top to bottom for cables  $c_9$ – $c_{12}$  (Fig. 2), respectively. Middle: ground contact information plotted for struts  $S_1$ ,  $S_2$  and  $S_3$  for 1000 ms. Dark portions of the lines indicate that a strut is in contact with the ground, and white portions indicate loss of ground contact. This gait is dynamic as it includes flight phases in which all four struts are off the ground at the same time. Bottom: configuration of the robot shown in three different phases of a gait cycle.

around time step 200, both cable forces show an increase, which is maintained for roughly the same duration of time  $\sim 100$  ms. Looking at the graph of foot contact, it can be seen that this time also corresponds to the time when the struts  $S_1$  and  $S_2$  come off the ground, followed shortly by strut  $S_3$ . Thus, the contraction of these two cables, while  $c_{10}$  is activated, causes the small hop. Labeling the cables  $c_9$ – $c_{12}$  as 1–4, respectively, the actuation pattern can be written as a loop through a sequence of binary states  $[s_1, s_2, s_3, s_4]$ , which for this gait is  $[0\ 1\ 0\ 0]$   $[1\ 1\ 0\ 1]$   $[1\ 1\ 1\ 1]$   $[0\ 0\ 0\ 0]$ .

The foot contact data in Fig. 12 are similar to Fig. 6 in that there are portions of the gait cycle in which all four struts are off the ground simultaneously. Thus, the gait here is also dynamic and similar to bounding. The gait is not perfectly periodic, although over a larger time scale an approximate periodicity can be observed. In the 1000 ms for which the forces and contact data are plotted, a little over four cycles are observed. Thus, the frequency of the gait cycle is roughly 4 Hz.

To provide further insight into the production of this dynamic gait in the TR-4, the configuration of the robot is shown at the bottom of Fig. 12 during three distinct phases of the gait cycle. Configuration A, which roughly corresponds to the take-off

phase, has cables  $c_9$  and  $c_{10}$  activated. Configuration B, which corresponds to the flight phase, has all four actuators activated. Configuration C, which corresponds approximately to stance phase, has only cable  $c_{10}$  activated. The movement of the robot using these changes in configuration can be seen in the sequence of still frames extracted from a video of the robot moving in Fig. 13.

The trajectory of the position of the center of mass of the robot is plotted in Fig. 14. The trajectory is more irregular than those produced by the TR-3 robot. One reason for this may be that the dynamics are more nonlinear as the system is more complex with a larger number of mass and spring elements.

## VI. FAULT TOLERANCE

As observed in Experiment 1 with the TR-4, the robot was able to produce gait without using one of its actuators. This indicated that the robot could demonstrate a certain degree of fault tolerance with respect to actuator damage. In order to further investigate fault-tolerant gait production, the TR-4 robot was tested with 1 and then two actuators damaged. Each condition was evaluated in ten experiments, where controllers were re-evolved for the remaining actuators. With one actuator damaged, the robot was still able to move and achieve fitnesses between 1.99–3.58 m with an average fitness of  $2.72 \pm 0.44$  m. With two actuators damaged, the robot was also able to move, although at a slower pace, with fitnesses ranging between 1.21–2.82 m, and an average fitness of  $1.98 \pm 0.62$  m.

Fig. 15(a) shows the cable force and ground contact data for a successful gait evolved in the single actuator damage condition. The fitness achieved in this experiment was 1.99 m in 10 s. One difference between this graph and the graph of cable forces in Fig. 12 is that the amplitudes of the forces are much higher. The graph suggests that the continued ability to produce gait relies on higher activation of the remaining cables to compensate for the lack of energy input from the inactive cable.

The ground contact data in Fig. 15(a) show a degree of periodicity almost as high as that observed in Figs. 6 and 12, which is significant considering that the robot is damaged. This suggests that the ability to produce a periodic gait is not significantly diminished due to this damage condition. The gait is also dynamic, similar to the gaits in Figs. 6 and 12. In fact, the flight phases of this gait last more than 50% of the gait cycle. This suggests that the ability to produce dynamic gait is also not significantly affected by the damage condition. The frequency of the gait is approximately 5 Hz, which is faster than that observed in Fig. 12. Thus, it seems that, in this case, using stronger cable contraction along with faster cycle times allows the robot to compensate for the lack of the fourth actuator.

Fig. 15(b) shows the graphs of cable forces and ground contact data for a successful gait evolved in the double-actuator damage condition. The fitness achieved in this experiment was 1.76 m in 10 s. Again, it can be seen that the amplitudes of the forces are higher than those in Fig. 12. However, the actuator  $c_{10}$  is only activated for a very short time during the gait cycle. Thus, the energy input into the system is significantly lower than the previous case.

The ground contact data in Fig. 15(b) show that the quality of the gait is more significantly affected by two actuators being

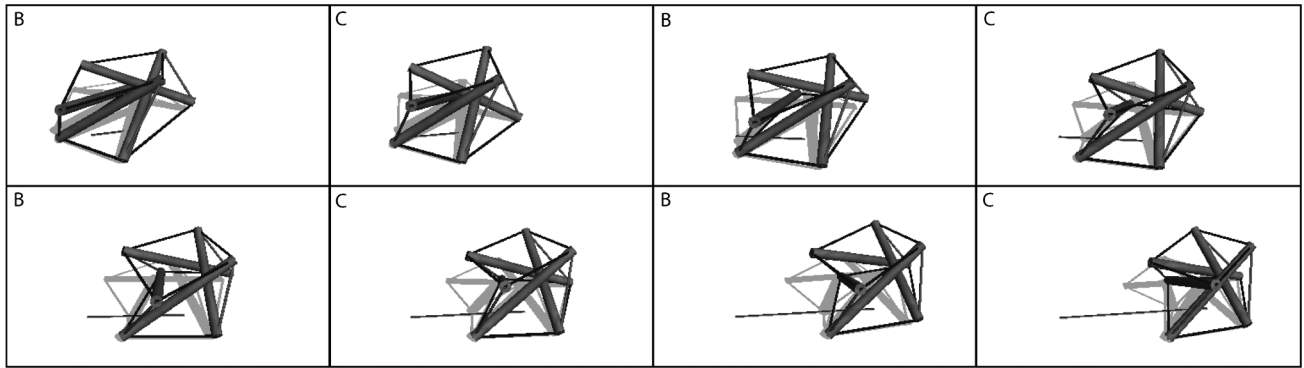


Fig. 13. Still frames extracted from video of the TR-4 robot locomoting in Experiment 5. The robot moves by alternating between flight phases while in configuration B and ground contact phases while in configuration C, both of which are depicted in Fig. 12.

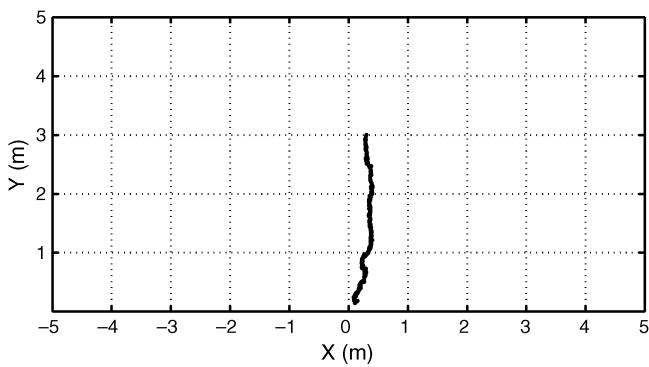


Fig. 14. TR-4, Experiment 5: the trajectory of the center of mass of the TR-4 robot is plotted for 10 s of operation time.

damaged. There is no apparent periodicity, and the gait pattern is irregular. The gait is also much more static, and there are no flight phases in which all four struts are off the ground at the same time. Nonetheless, as the fitness is 1.76 m, it would seem that the gait is exploiting another strategy, using low frequency cable contraction and moderate energy input to achieve some form of static gait.

Fig. 16(a) shows the trajectories of the center of mass of the robot in each of the ten experimental trials with one actuator damaged. On average, the trajectories seem to have a counterclockwise bias as in Figs. 11 and 14, but are more strongly curved. However, with appropriate feedback control, it may be possible to achieve straight line motion even with one actuator damaged. Interestingly, the more static gaits of Fig. 16(b) are less curved, although they are also shorter on average. Once again, it seems likely that, with control, it could be possible to harness the ability for locomotion for straight line motion.

As a final comparison, the fitnesses achieved in these experiments are plotted against the fitnesses of the experiments in which all four actuators are working, in Fig. 17(a). With one actuator damaged, the robot is able to produce gaits with an average speed of 0.27 m/s. With two actuators damaged, the robot is still able to produce gaits with an average speed of 0.20 m/s. The main consequence of actuator damage is a reduction in speed and not an inability to produce gait. One of the main reasons for the decline in speed is the reduction in energy input

into the system. With one actuator damaged, there is a 1/4th reduction in energy and, with two, it is 1/2. Normalizing the fitness by the number of actuators, as in Fig. 17(b), shows that the performance per actuator actually increases in the damage conditions, indicating that the decline in performance due to actuator damage represents a graceful degradation rather than a catastrophic failure.

## VII. PHYSICAL ROBOT

To test the feasibility of a tensegrity robot in the real world, a physical robot was built inspired by the TR-3 robot simulation (Fig. 18). Aluminum tubes were used for the struts, and nylon covered rubber elastic cable was used for the cables. The struts were 0.4 m long and the cables lengths  $S_1$  and  $S_2$  were 0.14 and 0.21 m at rest and 0.15 and 0.33 m in the equilibrium configuration. This led to a structure with overall length, width, and height of 0.36, 0.21, and 0.23 m, respectively. The overall weight of the structure was 680 g. The physical parameters of the physical robot were slightly different from those of the simulation: the struts were slightly heavier, the cables had slightly higher elasticity, and the floor had higher friction, due to our particular choice of materials and test environment. However, it was not considered particularly important to create an exact correspondence between the simulation and the real robot, but to develop a platform that would validate the feasibility of a tensegrity robot.

The pure linear actuation of the transverse cables in the simulation were approximated using Hitec HS-625MG servomotors mounted on the struts. The servomotor axle was fitted with a 2.54-cm plastic arm to which the cable was attached using a nut, bolt, washer fitting, and heavy duty fishing line. The motor had a range of motion of  $45^\circ$ . During walking, each servomotor was controlled to alternate between its maximum and minimum positions, producing an approximately 2-cm change in the length of the cable. The actuators were labeled as [1, 2, 3], where 1 corresponded to the servomotor towards the front of the image, 2 corresponded to the one in the middle at the top, and 3 corresponded to the one behind and on the bottom. When each actuator was at its minimum position so that the cable was at rest length, it was considered to be in state 0. When it was at its maximum position, exerting force on the cable, it was considered to be in state 1. A periodic pattern of actuation was used which corresponded to looping through the states in the following order

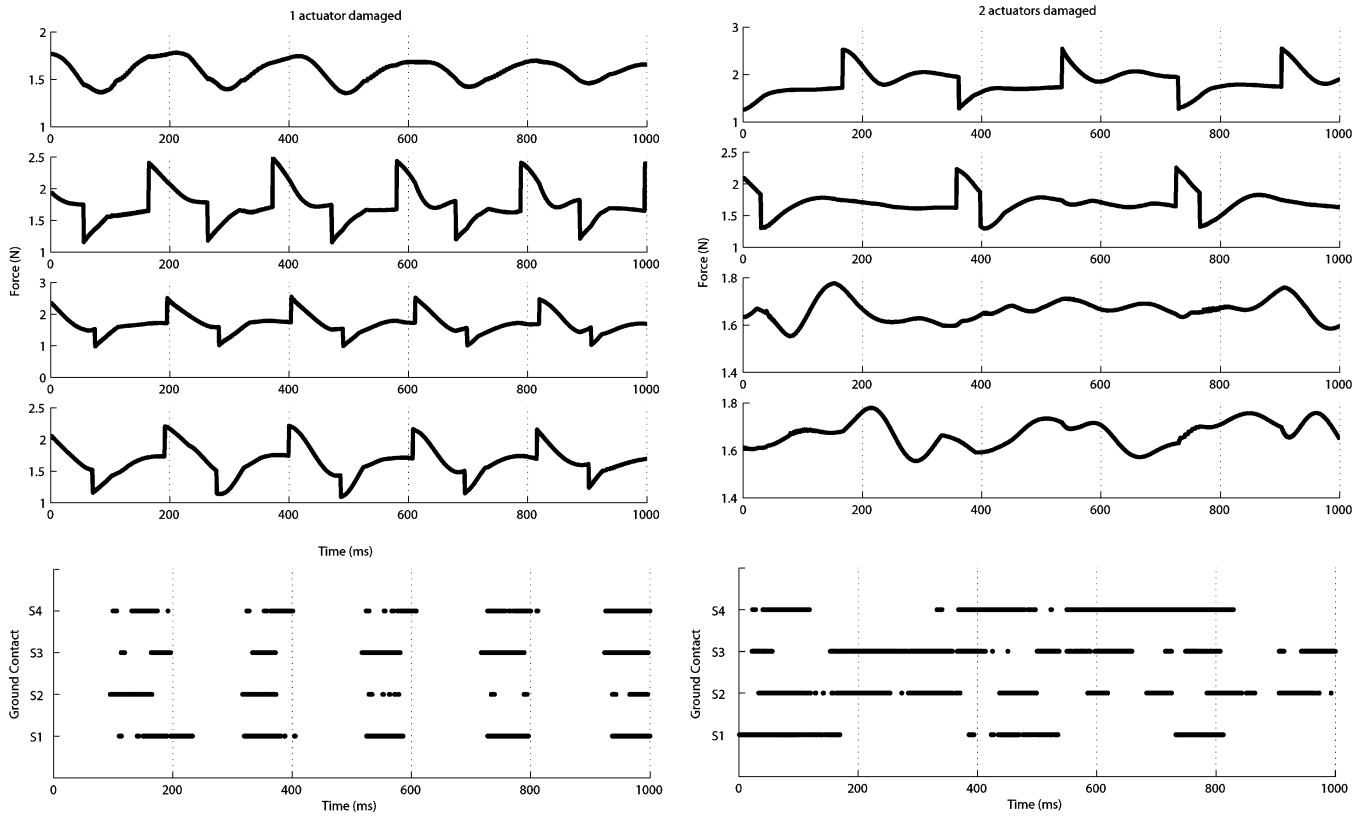


Fig. 15. Cable force and ground contact data of successful gaits produced with actuator damage, plotted for 1000 ms. (The arrows indicate the damaged actuators.) (a) One damaged actuator. (b) Two damaged actuators.

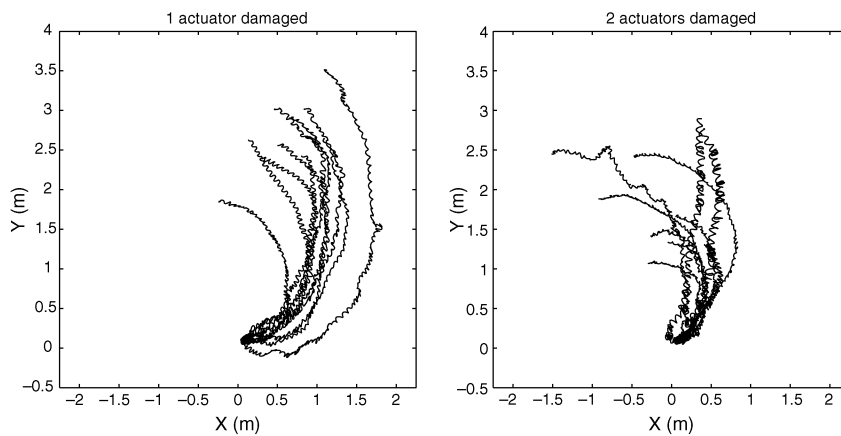


Fig. 16. (a) Trajectories of the position of the CoM of the robot, for the ten experimental trials with one actuator damaged, plotted for 10 s. (b) Trajectories of the position of the CoM of the robot, for the ten experimental trials with two actuators damaged, plotted for 10 s.

[1, 0, 0], [1, 0, 1], [1, 1, 0], [1, 1, 1], [0, 0, 0], [0, 0, 1], [0, 1, 0], [0, 1, 1]. Using this controller, the robot was able to produce gait in the longitudinal direction at a speed of 60 cm/min as seen in Fig. 19.

### VIII. DISCUSSION

#### A. Results

The use of evolutionary optimization to find periodic open-loop controllers for tensegrity robots in simulation yielded positive results. In all the experiments, controllers were designed

which led to nonzero movement of the center of mass over time (see Figs. 3 and 9). This suggests that the tensegrity structures implemented, with the particular physical parameters used, were highly capable of movement. This result is not entirely unexpected. As discussed in Section I, the elastic tendinous network which maintains the form of a tensegrity structure has a high potential for energy storage and release. The optimization algorithm could thus simply design a sequence of actuation patterns such that this energy would be released to produce motion in the desired direction. Nonetheless, the simulation results experimentally validate the hypothesis that tensegrity

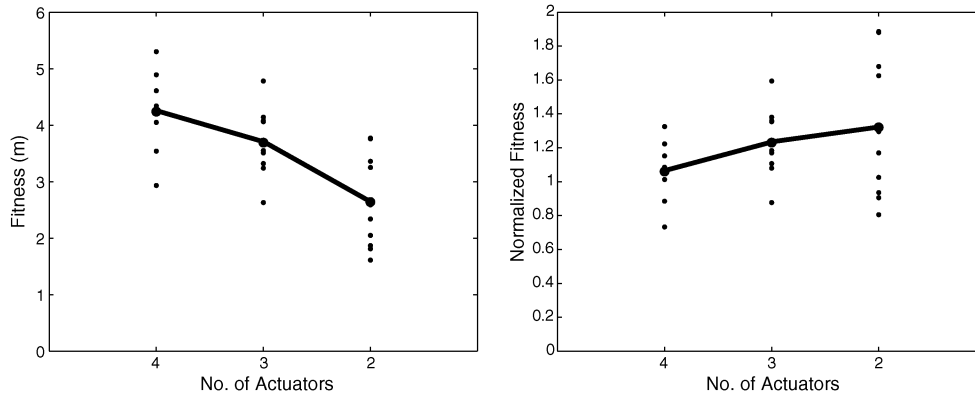


Fig. 17. Graceful degradation of locomotor performance in response to actuator failure. (a) Performance of the TR-4 robot with four, three, and two actuators active. The small dots represent the best fitness achieved in each experiment, and the large dot represents the average over all the runs in each condition. (b) Performance of the robot with four, three, and two actuators active normalized by the number of active actuators. The small dots represent the normalized fitness, and the large dot represents the normalized average over all of the runs.

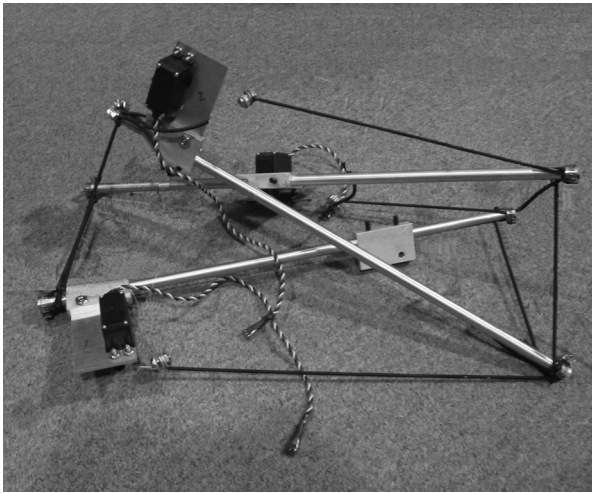


Fig. 18. Robot resembling TR-3 implemented in the real world.

structures are suitable for movement. The implementation of the real world robot provides physical evidence.

However, although all of the controllers produce motion approximately in the desired direction, not all the trajectories track a straight line. There are two possible reasons why this is the case. The first is that the evolutionary search for controllers does not directly reward for straight line motion. If an agent has a gait which is fast but slightly asymmetric, it may still achieve a better fitness than an agent with a slow straight gait, and thus, several of the agents opt for this strategy. The second reason why straight-line gaits are not commonly observed may be the bilateral asymmetry of the structures. Although the three- and four-strut tensegrity prisms were simple structures to start with, they may not have been the best structures possible for locomotion due to their inherent bilateral asymmetry. Tensegrity prisms are skewed by nature. The angle at which the top polygon is skewed from the bottom polygon depends on the number of struts in the structure [26]. This skew suggests that a pure periodic oscillation in the cables should lead to movement which is biased to one direction. Only with feedback-based correction would it be possible for such a structure to achieve perfect

straight line motion. Nonetheless, the fact that some of the trajectories are not too far from straight-line motion suggests that it would be possible to achieve with appropriate feedback-based control.

Another characteristic of the gaits found in the results were that they were not perfectly periodic, although the pattern of actuation applied in all cases was periodic. This effect is quite pronounced, for example, in the pattern of foot contacts in Fig. 4. Although approximately three periodic cycles of actuation are applied to the cables, there is less corresponding periodicity in the pattern of foot contacts. In the other gaits as well, although the periodicity is more apparent, it is not perfect. The reason for this is that the dynamics of the tensegrity structure, in intermittent contact with the ground, are defined by a second-order nonlinear hybrid system, and, in such systems, it is not always the case that periodic inputs produce periodic behavior. Furthermore, the genetic algorithm used here did not directly reward for periodicity in the fitness function, and thus the controllers were not required to satisfy this criterion. One way to improve the periodicity of the gait would thus be to explicitly reward for this in the fitness function. However, a more substantial improvement in periodicity would most likely be obtained using a controller architecture based on coupled oscillators. Such a controller would enable phase locking between the control inputs and the mechanical structure leading to a more stable limit cycle in the gait pattern [43], [48].

The simulation of both robots used relatively light struts and cables with low spring constants. This was shown to produce successful gaits. These physical parameters were selected partly due to the use of ODE's physics-based simulation, which posed some computational constraints. Large masses and forces could not be used, as with moderate calculation time steps of 0.001 s, positive feedback in the calculation of forces lead to instability in the system. For this reason, the masses of the struts as well as the spring constant of the cables had to be low. For higher masses or spring constants, the calculation time step had to be changed from 0.001 to 0.0001, which was ten times slower. For this reason, the masses and spring constants used were restricted to a range that would enable simulation at 0.001-s time steps and were lower than what would be expected in reality.

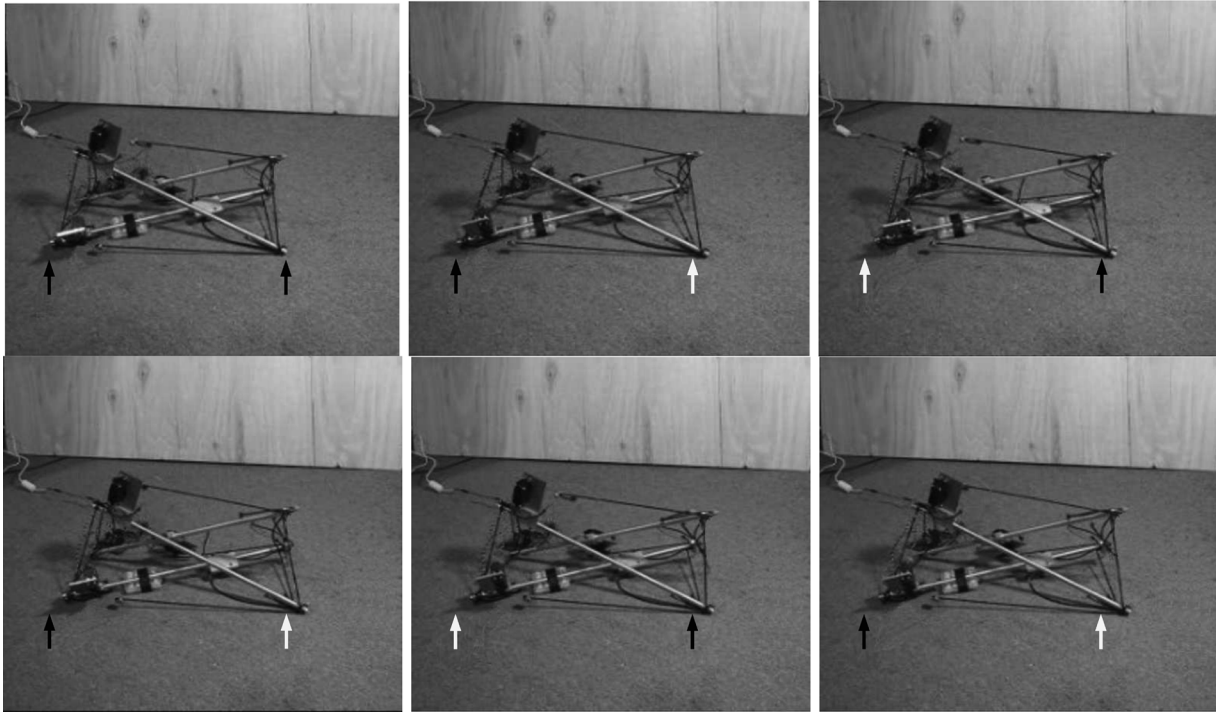


Fig. 19. Still frames extracted from video of robot walking. The robot walks by alternating forward movement in the two bottom struts. Arrows have been added to indicate the original location of the strut ends. The arrow is colored light to indicate which strut has just been moved.

How well the simulation results transfer to the real world is an important question. If the parameters of the simulation could be implemented exactly, then the behaviors observed in simulation would transfer to the robot in the real world. However, as the simulation experiments were performed before the construction of the real robot, physical properties of materials were not specifically considered in its design. Thus, the robot differed from simulation due to real-world factors such as actuator size, actuator placement, and available material properties for cables. Thus, it is not likely that the gaits observed in simulation would have identical counterparts in the real robot. Nonetheless, despite these differences, the gait presented in Section VIII is qualitatively similar to the slow gait evolved in simulation Experiment 4 with the TR-3 robot. A more accurate simulation could be achieved, of course, once a real robot exists. However, the challenge is to find realistic models for the physical parameters of the robot. This can be difficult for parameters such as spring and damping constants as spring constants of real materials are often nonlinear and include hysteresis, and damping constants are difficult to measure. Nonetheless, it would be possible to develop appropriate approximations which could be used to simulate the robot.

### B. Advantages and Disadvantages

In traditional robot design, the goal of control is to ensure that each joint is precisely controlled and tracks a desired joint trajectory, although the physical structure of a robot usually includes dynamic interactions between the motions of multiple joints. Thus, the control often seeks to decouple dynamic interactions between the individual joints. While such designs often lead to successful control strategies, from the perspective of the

mechanical structure, they are often not fault-tolerant. Thus, for example, in a quadruped robot, a broken knee joint may drastically impair the ability to produce gait. In a tensegrity robot, actuation at one location of the structure produces motion at multiple locations. The dynamics are even more coupled than in a traditional robot. This feature gives the structure a high degree of fault tolerance. If an actuator is damaged, another may be used to make up for its function. The utility of this feature was demonstrated in Section VII.

The fact that application of a force on one part of the structure causes a global deformation in the structure also presents other benefits. One actuator can be used to actuate multiple cables, which leads to the possibility for a small number of actuators to cause a global movement pattern and for multiple subsets of actuators to be used to produce the same behavioral outcome.

Tensegrity robots also have other advantages. They can be lightweight, due to the fact that the structure achieves its rigidity based on a high number of tensile elements and a relatively small number of rigid elements. Moreover, as only a small number of actuators are used relative to the number of degrees of freedom, this can lead to additional reduction in weight. Tensegrity robots also have a high strength-to-weight ratio and are effective at absorbing shocks.

In addition, tensegrity robots have the possibility for low-volume stowage, self-deployability, and reconfigurability. These are new features in the realm of robotics, which have not been easily achievable using conventional technology. While the utility of these features may be limited to certain application domains, they nonetheless broaden the range of possibilities for robots.

## IX. CONCLUSION

This paper introduced the concept of using tensegrity structures as the basis for land based locomotor robots. Two tensegrity robots, based on three- and four-strut tensegrity prisms, were designed in simulation. Using evolutionary optimization to obtain periodic gait controllers for these robots, it was demonstrated that such robots had the potential to generate various gait patterns. It was also demonstrated that the ability to produce gait in such structures was not drastically impaired by actuator damage, but showed a graceful degradation in locomotor ability. A physical robot was designed based on the three-prism tensegrity structure. This robot demonstrated the ability to produce forward locomotion, providing a real-world validation of the results from simulation. The results suggest that tensegrity structures can be used to form the basis of efficient, fault-tolerant, and physically robust robots for locomotion.

## REFERENCES

- [1] J. Albus, R. Bostelman, and N. Dagalakis, "The NIST robcrane," *J. Res. Nat. Inst. Sci. Technol.*, vol. 97, no. 3, pp. 373–385, 1992.
- [2] J. B. Aldrich, R. E. Skelton, and K. Kreutz-Delgado, "Control synthesis for a class of light and agile robotic tensegrity structures," in *Proc. IEEE Amer. Control Conf.*, Denver, CO, Jun. 2003, vol. 6, pp. 5245–5251.
- [3] R. Adhikari, R. E. Skelton, and W. J. Helton, "Mechanics of tensegrity beams" UCSD Struct. Syst. Control Lab., San Diego, CA, Rep. 1998-1, 1998.
- [4] M. Buehler, R. Battaglia, A. Cocosco, G. Hawker, J. Sarkis, and K. Yamazaki, "Scout: A simple quadruped that walks, climbs and runs," in *Proc. Int. Conf. Robot. Autom.*, 1998, pp. 1707–1712.
- [5] C. R. Calladine, "Buckminster Fuller's 'Tensegrity' structures and Clerk Maxwell's rules for the construction of stiff frames," *Int. J. Solids Struct.*, vol. 14, pp. 161–172, 1978.
- [6] A. Chassignoux, S. Chomarat, and J. Savel, "A study of morphological characteristics of tensegrity structures," *Int. J. Space Struct.*, vol. 7, no. 2, pp. 165–172, 1992.
- [7] R. Connelly and M. Terrell, "Globally rigid symmetric tensegrities," *Struct. Topol.*, vol. 21, pp. 59–78, 1995.
- [8] R. Connelly and A. Black, "Mathematics and tensegrity," *Amer. Scientist*, vol. 86, 1998.
- [9] C. J. Correa, "Static analysis of tensegrity structures," M.Sc. thesis, Dept. Mech. Eng., Univ. Florida, Gainesville, 2001.
- [10] H. Cruse, C. Bartling, J. Dean, T. Kindermann, J. Schmitz, M. Scumm, and H. Wagner, "Coordination in a six-legged walking system: Simple solutions to complex problems by exploitation of physical properties," in *Proc. 4th Int. Conf. Simul. Adapt. Behav.*, Cape Cod, MA, 1996, pp. 84–93.
- [11] B. de Jager and R. E. Skelton, "Input/output selection for planar tensegrity models," in *Proc. 40th IEEE Conf. Decision Control*, Orlando, FL, Dec. 2001, vol. 5, pp. 4280–4285.
- [12] B. de Jager, R. E. Skelton, and M. Masic, "Integrated control/structure design for planar tensegrity models," in *Proc. IEEE Int. Conf. Control Appl.*, Glasgow, U.K., Sep. 2002, vol. 2, pp. 862–867.
- [13] B. Domer, B. Raphael, K. Shea, and I. F. C. Smith, "A study of two stochastic search methods for structural control," *J. Comput. Civil Eng.*, vol. 17, no. 3, pp. 132–141, 2003.
- [14] J. Duffy, J. Rooney, B. Knight, and C. Crane, "An analysis of the deployment of tensegrity structures using screw theory," in *Proceedings of the Sixth International Symposium on Advances in Robot Kinematics: Analysis and Control*. Strobl, Austria: Kluwer, 1998.
- [15] R. Fuller, "Tensegrity," *Portfolio Artnews Annu.*, vol. 4, pp. 112–127, 1961.
- [16] R. B. Fuller, "Tensile-Integrity Structures," U.S. Patent 3 063 521, Nov. 13, 1962.
- [17] H. Furuya, "Concept of deployable tensegrity structures in space applications," *Int. J. Space Struct.*, vol. 7, no. 2, pp. 143–151, 1992.
- [18] A. Hanaor, "Tensegrity: Theory and application," in *Beyond the Cube: The Architecture of Space Frames and Polyhedra*, J. Francois Gabriel, Ed. New York: Wiley, 1997, pp. 385–408.
- [19] —, "Aspects of design of double layer tensegrity domes," *Int. J. Space Struct.*, vol. 7, no. 2, pp. 101–103, 1992.
- [20] K. Hirai, M. Hirose, Y. Haikawa, and T. Takenaka, "The development of Honda humanoid robot," in *Proc. IEEE Int. Conf. Robot. Autom.*, 1998, vol. 2, pp. 1321–1326.
- [21] G. S. Hornby, H. Lipson, and J. B. Pollack, "Generative encodings for the automated design of modular physical robots," *IEEE Trans. Robot. Autom.*, vol. 19, no. 4, pp. 703–719, Aug. 2003.
- [22] D. E. Ingber, "Architecture of life," *Sci. Amer.*, pp. 48–57, Jan. 1998.
- [23] —, "Cellular tensegrity: Defining new rules of biological design that govern the cytoskeleton," *J. Cell Sci.*, vol. 104, pp. 613–627, 1993.
- [24] N. Kanchanasaratool and D. Williamson, "Modelling and control of class NSP tensegrity structures," *Int. J. Control*, vol. 75, no. 2, pp. 123–139, 2002.
- [25] —, "Motion control of a tensegrity platform," *Commun. Inf. Syst.*, vol. 2, no. 3, pp. 299–324, 2002.
- [26] H. Kenner, *Geodesic Math and How to Use It*. Berkeley, CA: Univ. California Press, 1976.
- [27] B. F. Knight, "Deployable antenna kinematics using tensegrity structure design," Ph.D. dissertation, Dept. Mech. Eng., Univ. of Florida, Gainesville, 2000.
- [28] S. M. Levin, "The tensegrity-truss as a model for spinal mechanics: Biotensegrity," *J. Mech. Med. Biol.*, vol. 2, no. 3, pp. 375–388, 2002.
- [29] K. Linkwitz, "Formfinding by the 'direct approach' and pertinent strategies for the conceptual design of pre-stressed and hanging structures," *Int. J. Space Struct.*, vol. 14, no. 2, pp. 73–87, 1999.
- [30] K. A. McIsaac and J. P. Ostrowski, "Motion planning for anguilliform locomotion," *IEEE Trans. Robot. Autom.*, vol. 19, no. 4, pp. 637–652, Aug. 2003.
- [31] M. Mitchell, *An Introduction to Genetic Algorithms*. Cambridge, MA: MIT Press, 1996.
- [32] R. Motro, H. Nooshin, Ed., "Forms and forces in tensegrity systems," in *Proceedings of the Third International Conference on Space Structures*. Amsterdam, The Netherlands: Elsevier, 1984, pp. 180–185.
- [33] —, "Tensegrity systems: The state of the art," *Int. J. Space Struct.*, vol. 7, no. 2, pp. 75–84, 1992.
- [34] S. R. Oh, K. K. Mankala, S. K. Agrawal, and J. S. Albus, "Dynamic modeling and robust controller design of a two-stage parallel cable robot," in *Proc. IEEE Int. Conf. Robot. Autom.*, New Orleans, LA, 2004, pp. 3678–3683.
- [35] A. Pugh, *An Introduction to Tensegrity*. Berkeley/Los Angeles: Univ. California Press, 1976.
- [36] S. Pellegrino, "Mechanics of kinematically indeterminate structures," Ph.D. dissertation, Dept. Eng., Univ. Cambridge, Cambridge, U.K., 1986.
- [37] J. Pratt and G. Pratt, "Intuitive control of a planar bipedal walking robot," in *Proc. IEEE Int. Conf. Robot. Autom.*, Leuven, Belgium, 1998, pp. 2014–2021.
- [38] M. H. Raibert, *Legged Robots That Balance*. Cambridge, MA: MIT Press, 1986.
- [39] C. Ridderström, "Legged locomotion: Balance, control and tools—From equation to action," Ph.D. dissertation, Dept. Mach. Des., Royal Inst. Technol., Stockholm, Sweden, May 2003, 100 44.
- [40] B. Roth and W. Whiteley, "Tensegrity frameworks," *Trans. Amer. Math. Soc.*, vol. 265, pp. 419–446, 1981.
- [41] H. J. Schek, "The force density method for form finding and computation of general networks," *Comput. Methods Appl. Mech. Eng.*, vol. 3, pp. 115–134, 1974.
- [42] R. E. Skelton, J. P. Pinaud, and D. L. Mingori, "Dynamics of the shell class of tensegrity structures," *J. Franklin Inst.*, vol. 338, no. 2–3, pp. 255–320, 2001.
- [43] J. J. E. Slotine, W. Wang, and K. El Rifai, "Synchronization in networks on nonlinearly coupled continuous and hybrid oscillators," in *Proc. 16th Int. Symp. Math. Theory Netw. Syst.*, Jul. 2004, CD-ROM.
- [44] K. D. Snelson, "Continuous Tension, Discontinuous Compression Structures," U.S. Patent 3 169 611, Feb. 16, 1965.
- [45] C. Sultan, "Modelling, design and control of tensegrity structures with applications," Ph.D. dissertation, School Aeronaut. Astronaut., Purdue Univ., West Lafayette, IN, 1999.
- [46] C. Sultan, M. Corless, and R. E. Skelton, "Tensegrity flight simulator," *J. Guid., Control, Dyn.*, vol. 23, no. 3, pp. 1055–1064, 2000.
- [47] —, "Reduced prestressability conditions for tensegrity structures," in *Proc. 40th ASME Struct., Struct. Dyn. Mater. Conf.*, St. Louis, MO, Apr. 1999, pp. 2300–2308.
- [48] G. Taga, Y. Yamaguchi, and H. Shimizu, "Self-organized control of bipedal locomotion by neural oscillators in unpredictable environment," *Biol. Cybern.*, vol. 65, pp. 147–159, 1991.

- [49] G. Tibert, "Deployable tensegrity structures for space applications," Ph.D. dissertation, Dept. Mech., Royal Inst. Technol. (KTH), Stockholm, Sweden, 2002.
- [50] A. G. Tibert and S. Pellegrino, "Review of form-finding methods for tensegrity structures," *Int. J. Space Struct.*, vol. 18, no. 4, pp. 209–223, 2003.
- [51] N. Vassart and R. Motro, "Multiparametered form-finding method: Application to tensegrity systems," *Int. J. Space Struct.*, vol. 14, no. 2, pp. 147–154, 1999.
- [52] S. Vogel, *Cat's Paws and Catapults*. New York: Norton, 1998.
- [53] D. Williamson, R. E. Skelton, and J. H. Han, "Equilibrium conditions of a tensegrity structure," *Int. J. Solids Struct.*, vol. 40, no. 23, pp. 6347–6367, Nov. 2003.
- [54] D. Williamson and R. E. Skelton, "A general class of tensegrity systems: Geometric definition," in *Proc. ASCE Conf. Eng. Mech. 21st Century*, La Jolla, CA, May 1998, pp. 736–739.
- [55] M. Masic and R. E. Skelton, "Open-loop control of class-2 tensegrity towers," in *Proceedings of the 11th Smart Structures and Materials Conference*. Bellingham, WA: SPIE, 2004, vol. 5383, pp. 298–308.
- [56] C. Paul, H. Lipson, and F. J. Valero-Cuevas, "Evolutionary form-finding of tensegrity structures," in *Proc. Genetic Evol. Comput. Conf.*, Washington, DC, Jun. 2005, pp. 3–10.



**Chandana Paul** (M'04) received the B.S. degree in brain and cognitive sciences, and the B.S. and M.S. degrees in electrical engineering and computer science from the Massachusetts Institute of Technology, Cambridge, in 1996 and 1998, respectively, and the Ph.D. degree in computer science from the Artificial Intelligence Laboratory, University of Zurich, Zurich, Switzerland, in 2004.

Since 2004, she has been a Postdoctoral Researcher with the Mechanical and Aerospace Engineering Department, Cornell University, Ithaca, NY.

Her work has included numerous projects in robotics and artificial intelligence, in the areas of biped locomotion, legged locomotion, passive dynamics, evolutionary robotics, planetary rovers, and neuro-musculo-skeletal modeling. Her main interest lies in the investigation of the relationship between morphology and control in robots and biological organisms, with a particular focus on morphological computation.



**Francisco J. Valero-Cuevas** (M'99) received the B.S. degree in engineering from Swarthmore College, Swarthmore, PA, in 1988, the M.S. degree in mechanical engineering from Queen's University, Kingston, ON, Canada, in 1991, and Ph.D. degree in mechanical engineering from Stanford University, Stanford, CA, in 1997, respectively.

He is currently an Associate Professor with the Sibley School of Mechanical and Aerospace Engineering, Cornell University, Ithaca, NY, and an Associate Professor of Applied Biomechanics, Weill

Medical College, Cornell University. His research interests focus on combining engineering, robotics, mathematics, and neuroscience to understand organismal and robotic systems for basic science, engineering, and clinical applications.

Prof. Valero-Cuevas is a member of the IEEE Engineering in Medicine and Biology Society, the American and International Societies of Biomechanics, the American Society of Mechanical Engineers, the Society for Neuroscience, and the Society for the Neural Control of Movement. He has received Research Fellowships from the Alexander von Humboldt (2005) and the Wenner-Gren (2006) Foundations, the Post-Doctoral Young Scientist Award from the American Society of Biomechanics (2003), the Faculty Early Career Development Program CAREER Award from the National Science Foundation (2003), the Innovation Prize from the State of Tyrol in Austria (1999), a Fellowship from the Thomas J. Watson Foundation (1988), and was elected Associate Member of the Scientific Research Society Sigma-Xi (1988). He serves as an Associate Editor for the IEEE TRANSACTIONS ON BIOMEDICAL ENGINEERING.



**Hod Lipson** (M'98) received the B.Sc. degree in mechanical engineering and the Ph.D. degree in mechanical engineering in computer-aided design and artificial intelligence in design from The Technion—Israel Institute of Technology, Haifa, Israel, in 1989 and 1998, respectively.

Since 2001, he has been an Assistant Professor with the Mechanical and Aerospace Engineering and Computing and Information Science Schools, Cornell University, Ithaca, NY. Prior to this appointment, he was a Postdoctoral Researcher with

Brandeis University's Computer Science Department and a Lecturer with the Mechanical Engineering Department, Massachusetts Institute of Technology, where he conducted research in design automation. His research interests focus on computational methods for synthesizing complex systems out of elementary building blocks, and the application of such methods to design automation and their implication to understanding the evolution of complexity in nature and in engineering.